

Method to Achieving High-Power Microwaves in Air and Argon

Mladen M. Kekez

Abstract—The paper summarizes the results of the microwave generation in atmospheric air and argon at high pressure. The method how to proceed to achieving higher power level is presented. Two experimental setups were considered. Attention is paid to the interactions between the frequencies in the resonant cavity i.e., the coherence effect. The objective is to get reproducible data and the generation of the microwave emission at the single frequency to avoid the coherence effect. The electrons in the cavity are created by the electric field and by the photoionization, enabling the population inversion to be obtained. Because of the electron impact with N_2 in air, molecules cannot lose this energy by photon emission, their excited vibrational levels are metastable and live for a long time. The microwave pulse of long duration can be generated. The various radiation lines created in the resonant cavity are noted. To achieve high-power microwave emission, the resonant cavity has to be tuned to the more powerful line of the rotational and/or vibrational transition of molecules in air occurring at high frequency and not at 1-GHz frequency used in this study. A compact system could be achieved by using the high-frequency line. The study points out that the microwaves are produced through the amplification by stimulated emissions of electromagnetic radiation (maser action) in air and argon.

Index Terms—Coronas, microwave generations, photoionization and coherence effect, spark channel discharges.

I. INTRODUCTION

THIS paper is a continuation of the earlier studies [1], [2]. A maser is a device that produces coherent electromagnetic waves through amplification by stimulated emission. In high pressure gases, the maser exploits a rotational and/or vibrational transition of molecules and atoms. The frequency corresponds to the energy difference between two quantum energy levels of the species in the gain medium, which have been pumped into a nonthermal population distribution [3]. The emissions from the maser (like in the lasers) are stimulated and the radiations are emitted coherently.

In the lasers, the gain (amplification) implies the population inversion. The gain medium (molecular, atomic, and electronic) uses the population inversion. The laser radiation is produced at specific frequencies only and the radiation is independent on the size of the cavity.

In the masers, the radiation depends on the size of the cavity. The atomic hydrogen maser is a well-recognized maser device. The resonant cavity of the hydrogen maser is tuned precisely to the 1.420-GHz frequency [4]. This frequency corresponds to the amount of energy needed to reverse the spin of the

electron of the hyperfine transition of the hydrogen atoms and is equivalent to the photon energy of $5.8726 \mu\text{eV}$.

The main characteristic of the resonant cavity is described by the quality factor $Q(=f/\Delta f)$. Δf is the bandwidth of the cavity and f is the resonance frequency of the cavity. If Q is low, the gain (amplification of the signal) at resonance is small. The cavity does not discriminate sharply (reject the unwanted frequencies) between the resonant frequency of the cavity and the frequencies on either side of the resonance.

In most experiments, the microwave pulses may contain few frequencies in the domain covered by the quality factor Q of the resonant cavity. In general, the interaction between two signals of the same amplitude and of different frequency: f_1 and f_2 is presented [5]

$$\Delta F \times \Delta t = 1 \quad \text{where } \Delta F = \| f_1 - f_2 \| \quad (1)$$

where Δt is the time interval at which the resulting signal has zero value between the two consecutive interactions. Δt keeps repeating in time as long as the signals f_1 and f_2 are applied. In the literature, (1) is referred to describe the coherence effect.

Equation (1) can also be applied if the amplitudes of the signal: f_1 and f_2 are not of the same value and their temporal behavior is different in terms of the decay of amplitude in time.

Equation (1) is derived under the condition that the intensity of the signals is small enough and the interactions of the signals are not changing the background temperature of the matter through which they are propagating.

Using the PSPICE program a number of interesting features can be derived regarding (1). The coherence effect is manifested as the amplitude modulation in the time domain and two frequencies peaks in the domain of the fast Fourier transform (FFT) providing that f_1 and f_2 are separated far enough.

The energy in the two pulses entering the interaction is always larger than the energy in the resulting pulse following the interaction. Because the energy balance must be maintained, the other frequencies must be generated during the interaction to compensate for the energy imbalance.

To understand better these processes, it is useful to consider a single frequency microwave pulse i.e., of the duration $\Delta T = 20 \text{ ns}$ as shown in Fig. 1, frame A. The FFT trace of this waveform is given in Fig. 1, frame B. Fig. 1 was obtained using the PSPICE program.

The interesting feature about the FFT plot is that the central frequency at 1.080 GHz has the lobes with the first peak at 1.010 GHz on the left and the first peak at 1.150 GHz on the

Manuscript received March 16, 2017; revised May 10, 2017; accepted June 16, 2017. Date of publication June 30, 2017; date of current version August 9, 2017.

M. M. Kekez is with High-Energy Frequency Tesla Inc., Ottawa, ON K1H 7L8, Canada (e-mail: mkekez@magma.ca).

Digital Object Identifier 10.1109/TPS.2017.2717875

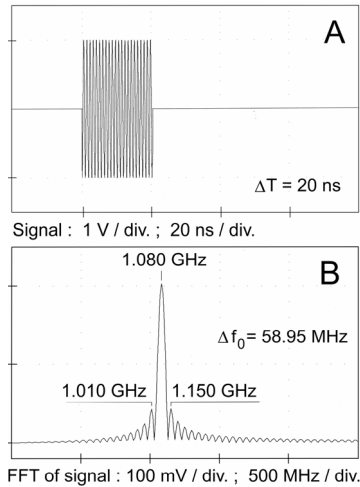


Fig. 1. Computer simulation. (a) Frame A is the PSPICE simulation of the waveform of the single frequency pulse. Duration of the pulse, ΔT is 20 ns. (b) Frame B is the FFT of this pulse. The rectangular window is used in definition of the FFT. Δf_0 is the FWHM of the frequency at 1.080 GHz.

right. If the additional signal with moderately high amplitude and of the frequency close to the peak at 1.080 GHz would interact with the main signal at 1.080 GHz, these lobes will have some change. To detect the presence of this additional signal, it is necessary to observe carefully the deformation of the lobes and to note the deflection point being present in the FFT curve close to the peak at 1.080 GHz.

Using the PSPICE program, it is also found that for the pulses of rectangular shape, the following relation holds:

$$\Delta T \times \Delta f_0 \leq 1.2 \quad (2)$$

where Δf_0 is the full width at half maximum (FWHM). Equation (2) can be used for the pulses of short duration, ΔT ranging from 10 ns to i.e., 80 ns that contain the single frequency in the pulse of the domain from 1 to 10 GHz.

If the amplitude of the single frequency pulse would decay rapidly in time, Δf_0 will rise and (2) cannot be applied any longer.

The purpose of this paper is to try to understand why in addition to the main frequency, other frequencies are present in the domain governed by the quality factor of the resonant cavity. The objective is to understand how to generate only the single frequency emission to exit the cavity. However, the main goal is to learn how to achieve the high-power level of the microwave generation in air.

II. EXPERIMENTAL SETUP AND RESULTS

The experimental setup used is shown in Fig. 2. The same setup was applied in [1] and [2].

The diagnostic tools are 10-GHz B-dot probe to measure the radiation exiting the device, Tektronix CT-1 transformer/probe to measure the electrical current in the cavity and 3-GHz Tektronix oscilloscope: TDS 694C to record the data.

B-dot probe records the radiation exiting the setup. The probe was calibrated in the TEM cell. For a frequency of 1.08 GHz, the amplitude of the signal of 1 V corresponds to

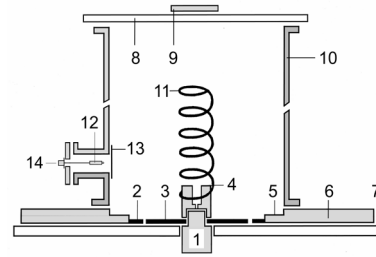


Fig. 2. Schematic of the experimental setup. 1–HV output from the nine-stage Marx generator, 2–copper ring, 3–copper plate, 4–metallic holder that provides the contact to nine-stage Marx generator, 5–step in the metallic flange, 6–metallic flange is connected to the enclosure of nine-stage Marx generator, 7 and 8–Plexiglas flanges, 9–partial reflector, 10–cylinder, 11–helix, 12–Tektronix CT-1 probe placed into 2 3/4 in nipple, 13–copper mesh, and 14–BNC connector. B-dot probe is placed above the partial reflector.

the electric fields of 3.07 kV/cm. The amplitude of the signal is linearly proportional to the frequencies in the range from 1 to 10 GHz.

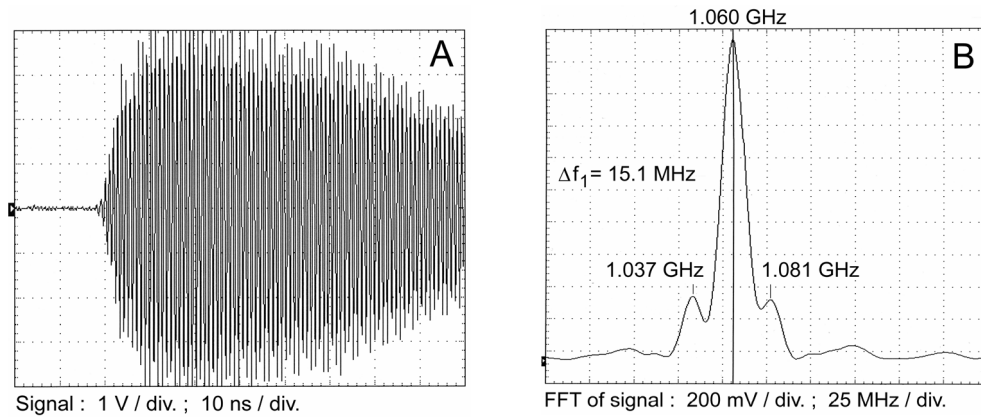
In Fig. 3(a), the average height of the signal is ≈ 4 divisions = 4 V. The average field E is 4 div. \times 3.07 kV/cm/div. = 12.28 kV/cm and the power density is $E^2/(2 \times 377\Omega) \approx 0.2$ MW/cm². The area of the radiation exiting the cavity, $A = \pi \times r^2 = 182.4$ cm², where $r = 3$ inch (=7.62 cm). When the measurements of the power density distribution over the area, A are done, it will be possible to specify how many (tens of) megawatts the setup in Fig. 2 is producing.

In zero order approximation, the setup in Fig. 2 could be considered as RLC resonant circuit/cavity that can discriminate/rejects the frequencies located away from the resonant frequency on either side of the resonance. This feature is described by the quality factor Q of the resonant cavity. B-dot probe records only the processes in the domain dictated by the quality factor Q of the resonant cavity.

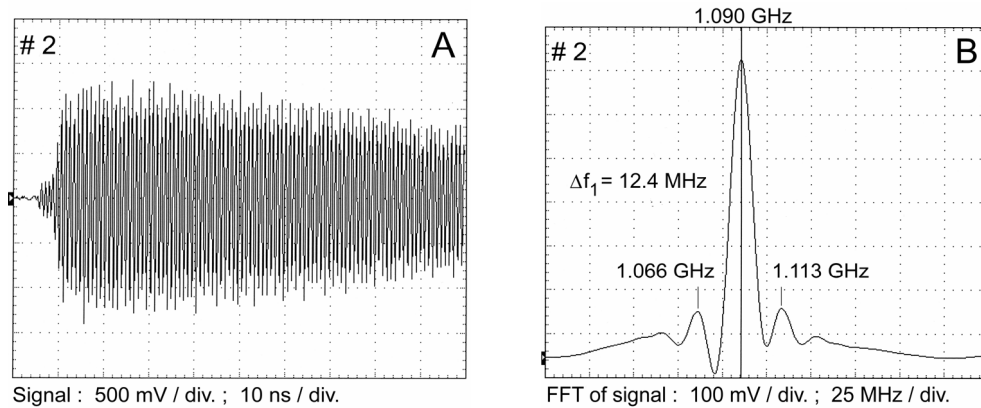
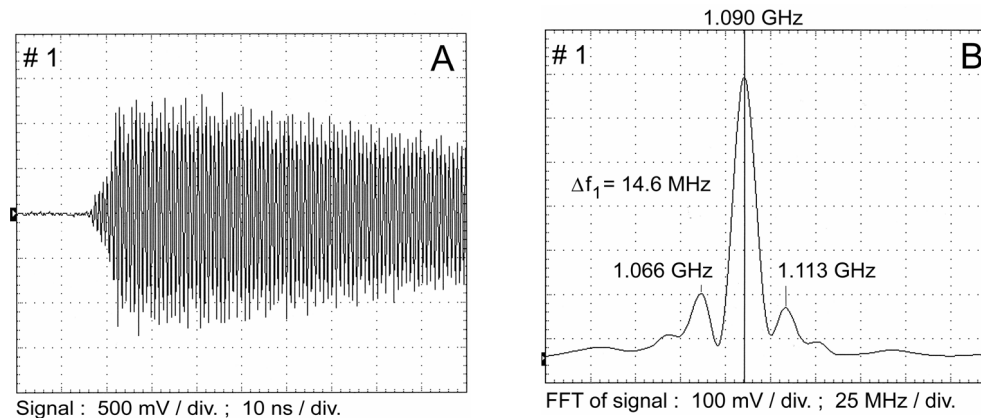
Tektronix CT-1 transformer/probe is used to obtain the current waveform. The frequency domain of the probe is from almost dc to 3 GHz. The amplitude of the signal recorded depends on the orientation of the probe in regards to the magnetic field.

The calibration of the CT-1 probe was done with the aids of Rogowski coil made by Pearson Electronics Inc., Model 110. “100 mV”/div recorded by the CT-1 probe corresponds to 667 A/div. The bandwidth of the CT-1 probe is used to record all the current waveforms presented, except the current data given in Fig. 6 where the filter was used. The bandwidth of the filter is from 300 MHz to 3 GHz.

Both probes observe mainly the radiations coming from the exited molecules and atoms in the RF and the microwave domain. These radiations are considered to be the electromagnetic waves and the probe measures the magnetic field arising from these radiations. The CT-1 probe records well the magnetic field of the radiations being generated close to the probe in the space between the cylinder 10 and the helix 11 (Fig. 2). The sensitivity of the probe is decreased for the radiations occurring inside the helix due to the geometrical distance of these radiations with respect to the probe. The CT-1 probe



(a)



(b)

Fig. 3. (a) Microwave emissions generated in air. These data are after [6] Fig. 7. The helix was used. Marx generator was charged to ~12 kV/stage. (b) Two shots of microwave emissions generated in argon at 700 torr. Marx generator was charged to ~10 kV/stage. Solid rod of 48.30 mm in diameter replaced the helix. The signals in frame A were recorded with B-dot probe together with a low (1.25 GHz) pass filter. Frame B is the FFT of the signal. Δf_1 is the FWHM of the frequency at the resonance. Coherence effect is absent.

records all the radiation lines being produced in the resonant cavity from the virtually dc to 3 GHz (=bandwidth of the oscilloscope)

To appreciate how the setup shown in Fig. 2 works, let us first note that when the helix is removed and nine-stage Marx generator is energized; the breakdown discharge takes place between the copper plate 2 and copper ring 3. The breakdown occurs in millimeter and submillimeter gaps over

the dielectric (Plexiglas) substrate. The gap is subject to high (few MV/cm) fields. The spark discharges are creating the uniform and rapid Ultra Violet (UV) photoionization in the volume of gas placed inside the cylinder 10 of Fig. 2, as discussed in [6].

When the helix is attached, the voltage across many spark channels created on the circumference of the plate 3 has not fallen to fully zero value. The part of the voltage pulse

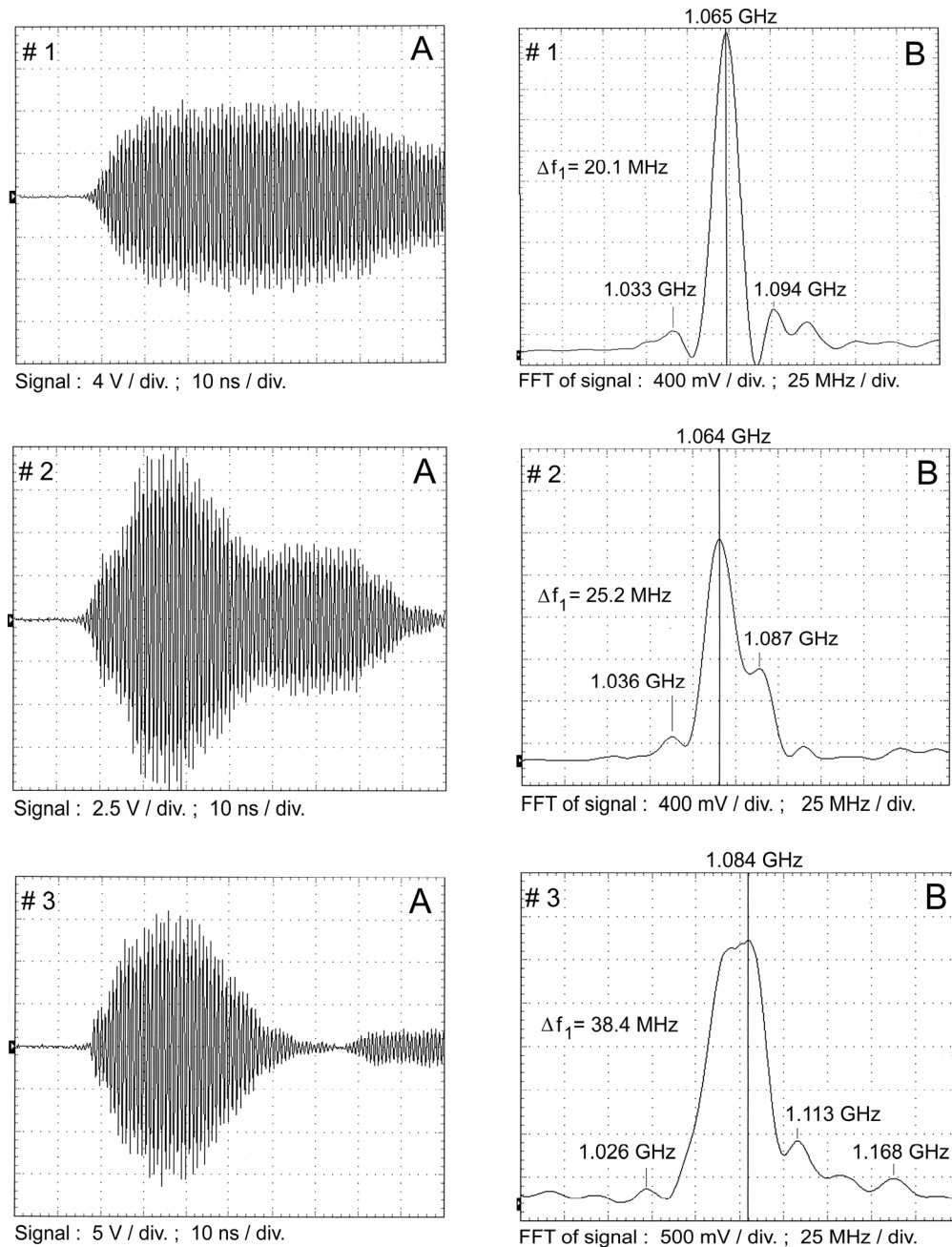


Fig. 4. Microwave emissions generated in air. The shots # 2 and # 3 are the records of “poor shots” of microwave emissions. The coherence effect is present in these two shots. Shots # 1 and # 3 have been recorded in the same run. The helix was used. Marx generator was charged to ~ 12 kV/stage. Descriptions of the traces are as in Fig. 3. The signal was recorded with B-dot probe together with a low (1.25 GHz) pass filter.

from the generator will traverse between the helix and the cylinder until it reaches the end of the helix. The wave will see the open circuit and will reflect back toward the electrode. There, we do not have the matching impedance condition and the wave will travel forth and back along the helix creating the electron impact ionization in the space between the helix and the cylinder. The electric field of the voltage pulse is well below the voltage breakdown potential.

The UV preionization provides and maintains the necessary ionization in the gas to carry the current and provides electrical

excitation of the molecules. The plasma produced by the UV preionization is also augmented by the applied electric fields via the Townsend multiplication parameters (defined via the parameter related to the ratio between the electric field and the neutral gas density) together with the parameters related to the high-speed (runaway) electron production.

The amplitude of the electric field on the helix depends on the value of the charging voltage of the Marx generator and on the spacing between the copper plate 2 and copper ring 3. To get the maximum value of the radiation exiting the cavity, it was learned that the Marx generator has to be charged to

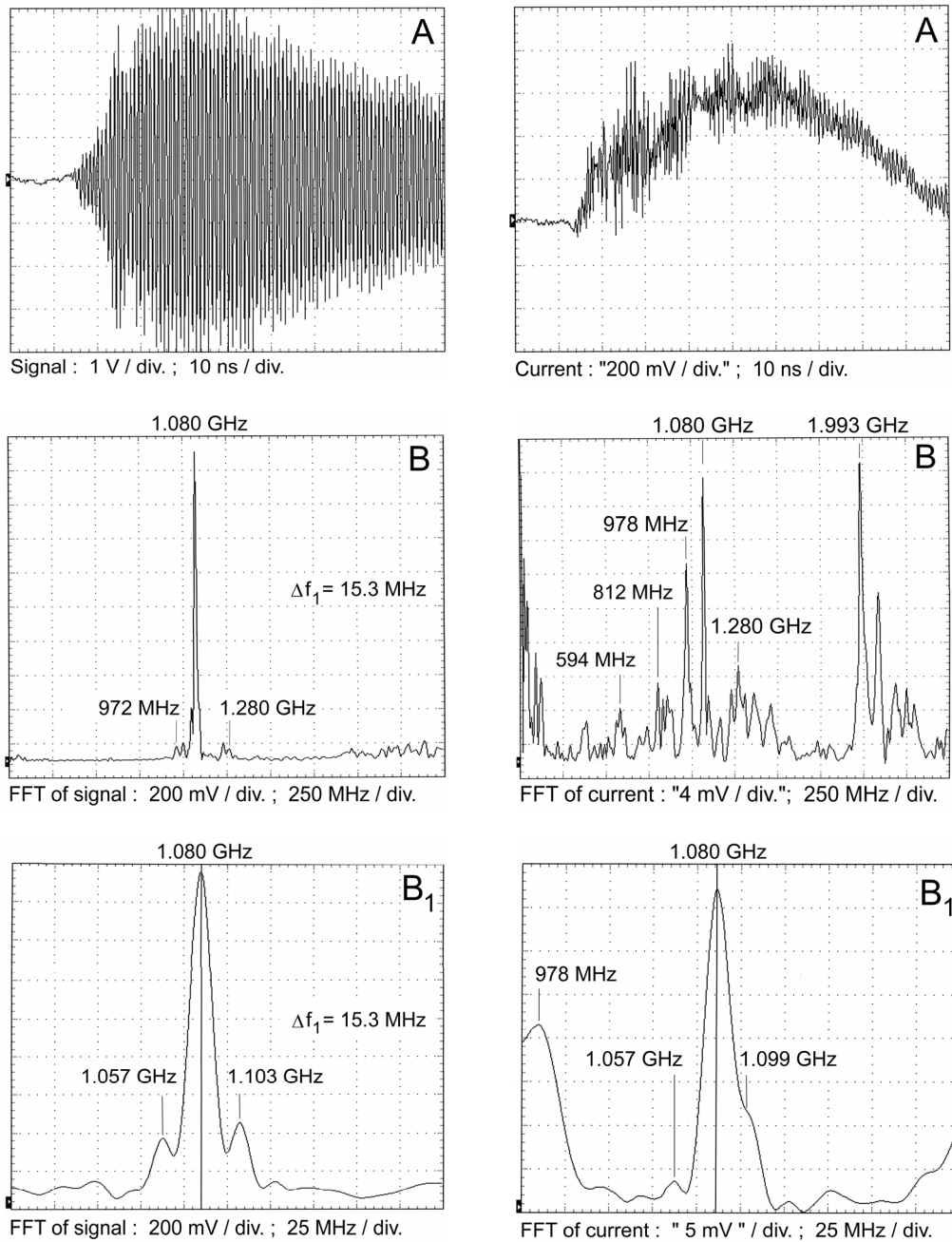


Fig. 5. Microwave emissions generated in air. The helix was used. The signal in (A) was recorded with B-dot probe to cover the domain from low megahertz domain to 3 GHz (=bandwidth of the oscilloscope). Current in frame A was obtained with Tektronix CT-1 current probe. Frames B are the FFT of the signal and of the current, respectively. Frame B₁ is expanded FFT of B. Δf_1 is the FWHM at frequency of 1.080 GHz. Marx generator was charged to ~12.5 kV/stage. Coherence effect is absent.

the particular (optimum) value. If the charging voltage is a few kilovolts above the optimum value, the voltage across the spark channels will fall causing the decrease of the current flowing between the helix and the cylinder up to a factor of 2, resulting in the decrease of the ionization and excitation of the constituencies in the gas by the electric field. If the Marx generator is charged to slightly lower voltage in comparison to the optimum value, the trace of the radiation emission will have the steps at the beginning of the emission, as shown in [7, Fig. 2].

The results obtained could be classified in two categories: “good data” where the system produces the radiation mainly at the single frequency, and “bad data” where in addition to the single frequency the satellite lines on one of the side or both sides of the single frequency are present.

A “good data” are shown in Figs. 3, 5, 11, 13 and 14, where the system produces the radiation at the single frequency. Similar to the data in Fig. 3(a), hundreds of “good shots” were also recorded, not only just in air but also in argon/SF₆ mixture [7]. It is interesting to note that the

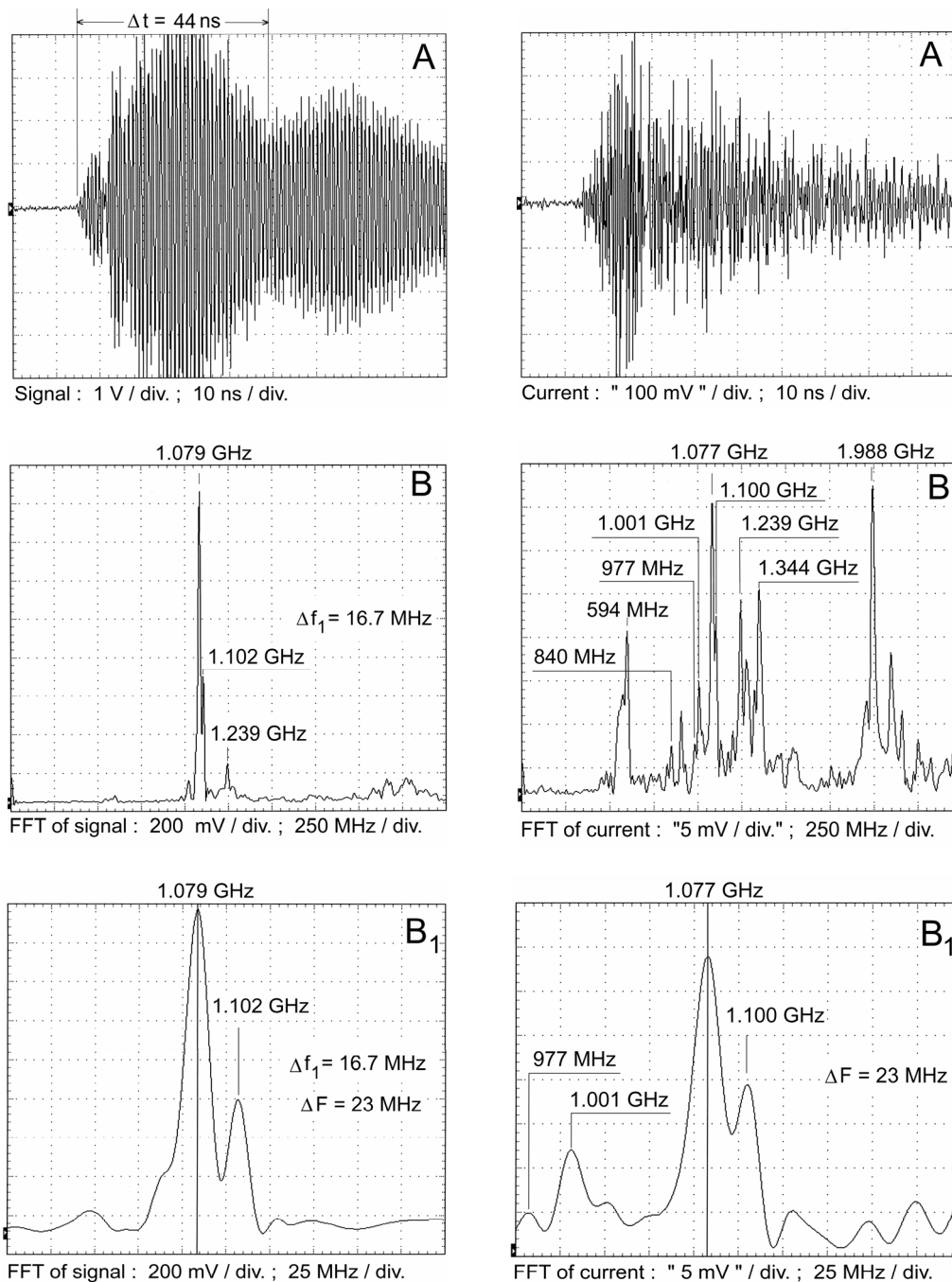


Fig. 6. Microwave emissions generated in air. The helix was used. Marx generator was charged to ~ 12 kV/stage. Descriptions of the traces are as in Fig. 5. Current in trace A was recorded using Tektronix CT-1 current probe and the filter to cover the bandwidth from 300 MHz to 3 GHz. Coherence effect is present.

resonant frequency had varied from 1.060 to 1.071 GHz from shot to shot [7]. The emission was circa two times large in amplitude in the argon/SF₆ mixture in comparison to the emission recorded in air. The puzzling fact was that in many series of 12 shots per run, for no obvious reason, the “bad shots” (Fig. 4, shot # 2 and shot # 3) were also recorded in addition to the “good shots” (for example in Figs. 3 and 5).

The satellite line is present on the right of the resonant frequency in Fig. 6, and we have a major interaction between the main frequency of 1.079 GHz and the satellite line at 1.102 GHz as shown in Fig. 6, frame B₁ of the signal. These two

lines are creating the coherence effect which is evaluated and given in Table I.

The satellite line at 1.057 GHz is present on the left of the resonant frequency of 1.082 GHz in Fig. 8, frame B₁ and Fig. 9, frame B₁, and the satellite line at 1.060 GHz is next to the main frequency line at 1.083 GHz in Fig. 10, frame B₁.

Seven examples of the interactions between the frequencies were presented in [8] and the comparison was made between the theory and the experiments. Attention was paid to observe the transient time for the wave to propagate in the cavity. To improve the quality of the analysis, the same experimental data was used again and the amplification by stimulated

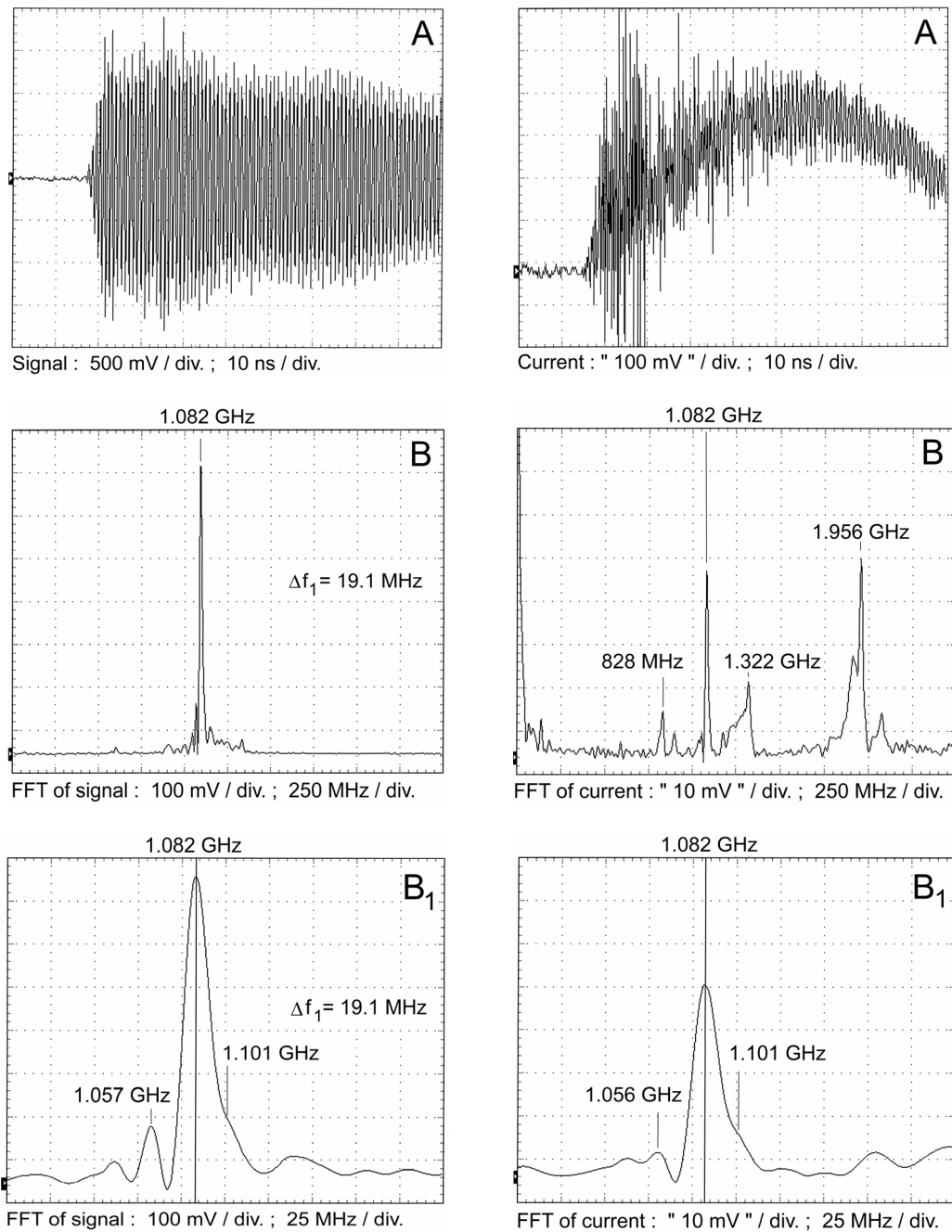


Fig. 7. Microwave emissions generated in argon at 600 torr. The helix was used. Marx generator was charged to ~ 9 kV/stage. The signal in frame A was recorded with B-dot probe and with low (1.25 GHz) pass filter. Other descriptions of traces are as in Fig. 5. Deflection point at 1.101 GHz contributes that the coherence effect is not absent, but the coherence effect is semiabsent or it could be stated that the effect is semipresent.

emissions of electromagnetic radiation (maser effect) was included in the theoretical formulation [9].

To examine the validity of the (2), two shots of the emissions in argon are presented in Fig. 3(b). The FFT data of the signal displayed on 25 MHz/div. closely follows the FFT trace shown in Fig. 1. In Fig. 3(b) shot # 1, the product of the signal duration of (≈ 78 ns) times Δf_1 of 14.6 MHz is ≈ 1.14 and this is in accordance with (2). Similarly, in the shot # 2 of Fig. 3(b) the product of the signal duration of (≈ 91 ns) times Δf_1 of 12.4 MHz is ≈ 1.13 .

The same conclusion can be reached regarding the data given in Fig. 3(a), frame B. The FFT data of the signal displayed on 25 MHz/div. is similar to the FFT trace shown in Fig. 1. The product of the signal duration of (≈ 78 ns) times Δf_1 of 15.1 MHz ≈ 1.18 , also agrees well with (2). The same statement can be made regarding Fig. 5.

To increase the probability of getting the “good shots,” the following procedure was used. After 12 shots were fired, the chamber was pumped down to 10^{-4} torr and fresh air was introduced. The idea was to remove the ozone and other

TABLE I

DATA OF FIGS. 6–10 ARE COMPARED WITH THEORY: $\Delta F \times \Delta t = 1$

	Frequencies (GHz)		ΔF (MHz)	Δt (ns)	$\Delta F \cdot \Delta t$	Difference from $\Delta F \cdot \Delta t = 1$
	Upper	Lower				
Fig. 6	1.102	1.079	23	44.0	1.012	+ 1.20 %
Fig. 8	1.082	1.057	25	41.4	1.035	+ 3.50 %
Fig. 9	1.082	1.057	25	41.8	1.045	+ 4.50 %
Fig. 10	1.083	1.060	23	43.1	0.991	-0.87 %

byproducts due to the spark channel breakdown created on the circumference of the plate 3. Unfortunately, this procedure did not yield the significant improvement in getting always the “good shots.”

After numerous trials of what to do, it was learned that the gap spacing between the plate 3 and the ring 2 of Fig. 2 was the pertinent fact. The gap has to be of a particular value in submillimeter range and be uniform around the circumference. Also, the Marx generator has to be charged only to ± 2 kV up and down around the optimum value of 12.5 kV/stage to get the “good results.”

With the introduction of the CT-1 probe in the experimental setup, it became possible to understand better what contributes to making the difference between the “good shot” (Fig. 5) and the “bad shot” (Fig. 6).

To learn more, further detailed studies were done in argon. “Semigood shot” using 10 ns/div. time scale is given in Fig. 7 and the “good shot” recorded on 20 ns/div. time scale is shown in Fig. 11. The term “semi-good shot” is used because the FFT plot of the signal shown in Fig. 7, frame B₁ has the satellite line of small amplitude next to the peak at 1.082 GHz, which results in the formation of the deflection point at 1.101 GHz.

From a few hundreds of the “bad shots” Figs. 8–10 have been chosen to show the progressive increase in the amplitude of the satellite line at 1.057 GHz shown in Figs. 8 and 9 and 1.060-GHz satellite line in Fig. 10. To appreciate the difference of the “bad shot” of Fig. 10, the “good shot” is given in Fig. 11.

When the helix was replaced by the solid graphite rod of 2 inch (=50.80 mm) in diameter, Figs. 12–14 were obtained.

The far end of the rod was machined to form the hemisphere. The reproducibility in generating the “good shot” of the microwave emissions became good. The importance of the precise gap spacing between the plate 3 and the ring 2 of Fig. 2 was reduced. For example Fig. 12 was obtained for the smaller spacing in comparison to that used in Figs. 13 and 14. Note that the solid aluminum rod of slightly smaller diameter of 48.30 mm was applied to get the results shown in Fig. 3(b).

III. DISCUSSION

The first step in the understanding of the results obtained is to evaluate the coherence effect described by (1). The comparison between the theory and the experimental findings is given in Table I.

TABLE II

COMPARISON BETWEEN THEORY AND EXPERIMENTS

Theory states that for N : and for the position in the space, the frequency is:	Not in the center $N = 2$	Not in the center $N = 3$	Center, $N = 2$
Experimental data Fig. 5	812	1.280	978
Experimental data Fig. 6	840	1.239	977
Experimental data Fig. 7	828	1.322	
Experimental data Fig. 8	828	1.322	
Experimental data Fig. 9	828	1.326	
Experimental data Fig. 12		1.243	
Experimental data Fig. 14		1.268	

An attempt is now made to understand why the frequency lines have been recorded in the current waveforms. The definition of the spatial resonator can help. The spatial resonator is defined as the distance d times 2 is equal to the integral number of wavelengths λ of the wave

$$2 \times d = N\lambda, \text{ where } N \text{ is the integral number } = 1, 2, 3 \dots \quad (3)$$

The distance between the partial reflector 9 and the copper plate 3 of Fig. 2 d is 36.4 cm. When the dimension of 36.4 cm is inserted into (3), for $N = 2$, the theoretical value of the frequency is 825 MHz and it is shown in the first row in Table II. In the second row in Table II, the theoretical frequency of 1.236 GHz is noted for $N = 3$.

To understand why the experimental value differs from the theoretic value, it is useful to consider Fig. 12. Next to 1.234 GHz line, there are two additional lines at 1.278 and 1.336 GHz. It appears that these two additional lines inhibit the observation of the theoretical frequency of 1.236 GHz in Figs. 7 and 8.

Table II shows that the experimental value of the frequency varies from shot to shot. This deviation could be explained by observing the details of the geometry. There is the small step, 5 of about 2 mm between the copper ring 2 and the aluminum flange 6 shown in Fig. 2. This step introduces uncertainties in the determination of the theoretical value of the frequency. This step is not included in the analysis. The term “not in the center” is used to observe the distance between the partial reflector and the copper plate.

The standing wave is also formed simultaneously between the top edge of the metallic holder 4 and the partial reflector 9. By measuring this distance and using (1) the frequency of 972 MHz was calculated for $N = 2$. This frequency is noted by the term “center” in Table II. Again, there are some uncertainties. The metallic holder 4 for the helix has the recess needed to provide the space to accommodate the screw that

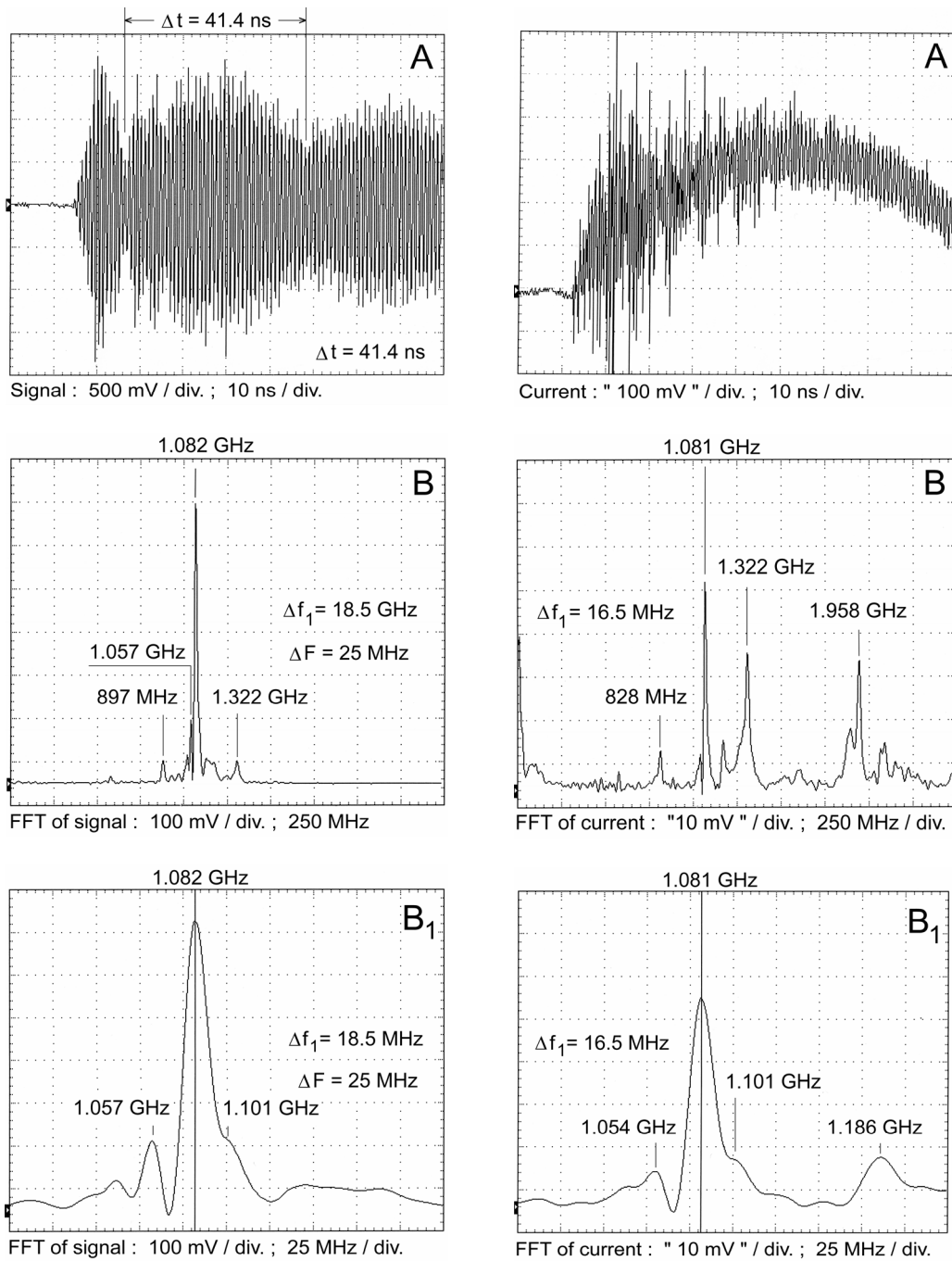


Fig. 8. Microwave emissions generated in argon at 600 torr. The helix was used. Marx generator was charged to $\sim 9 \text{ kV}$ /stage. The signal in frame A was recorded with B-dot probe and with a low (1.25 GHz) pass filter. Other descriptions of traces are as in Fig. 5. Coherence effect is present.

is joining the metallic holder 4 to the bushing of the Marx generator 1 shown in Fig. 2.

The frequency peak at 594 MHz was observed in Fig. 6 and this peak is absent in Fig. 5. The peak at 594 MHz can be contributed to the coherence effect. In Table I, it has already been pointed out that the main frequency at 1.079 GHz interacts with the satellite line at 1.102 GHz to cause the coherence effect. As stated in Section I, the coherence effect will in turn create the additional frequencies such as 1.001 GHz and 594 MHz (Fig. 6) to preserve the energy balance between the

pulses entering the interaction with the energy in the resulting pulses following the interaction.

100 % modulation of the signal is present in Fig. 10. The coherence effect is also manifested by the establishment of the peak at the frequency of 546 MHz. There are two possible interpretations for the experimental finding given in Figs. 6 and 10. The first interpretation is to take that these are the true low-frequency components of the current occurring at 594 MHz in Fig. 6, frame B and 546 MHz in Fig. 10, frame B. The second possible interpretation is to note that the oscilloscope has only

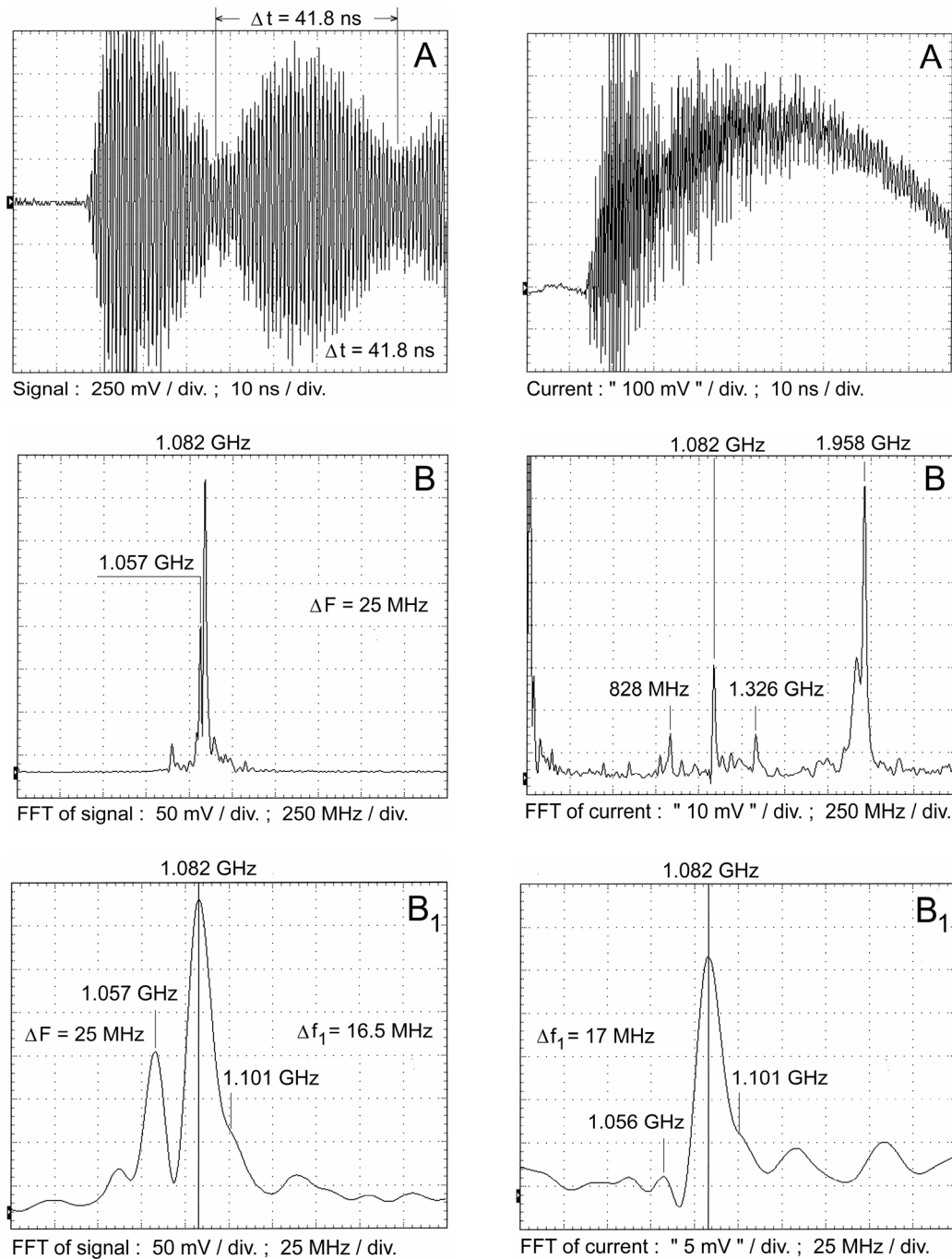


Fig. 9. Microwave emissions generated in argon at 600 torr. The helix was used. Marx generator was charged to ~ 9 kV/stage. The signal in frame A was recorded with B-dot probe and with a low (1.25 GHz) pass filter. Other descriptions of traces are as in Fig. 8. Coherence effect is present.

the bandwidth of 3 GHz and the oscilloscope interprets high-frequency signals well above 3 GHz as the low-frequency data. This uncertainty can be resolved by the use of a faster (i.e., 32 GHz) oscilloscope.

The frequency line close to 1.9 GHz is observed in all the data of the emissions recorded in air. It ranges from 1.950 shown in Fig. 14 to 1.993 GHz given in Fig. 5. This 1993-GHz line becomes 1.958-GHz line in argon as shown in Figs. 8 and 9. It can be taken that this high-frequency line is due to the rotational and/or vibrational transition of molecules

present in the microwave domain in air and argon. The same statement can be made regarding the line at 1.336 GHz recorded in air and shown in Fig. 12 and the line of 1.322 GHz observed in argon and shown in Fig. 8.

The frequencies exiting the oscillatory circuit/system (Fig. 2) can be considered as coming from the coaxial waveguide. As shown in [1], [2], and [10], the experimental evidence points out that the TE_{11} mode predominates in the experimental setup (Fig. 2). The TE_{11} (peak-on axis) mode has the smallest cutoff frequency value

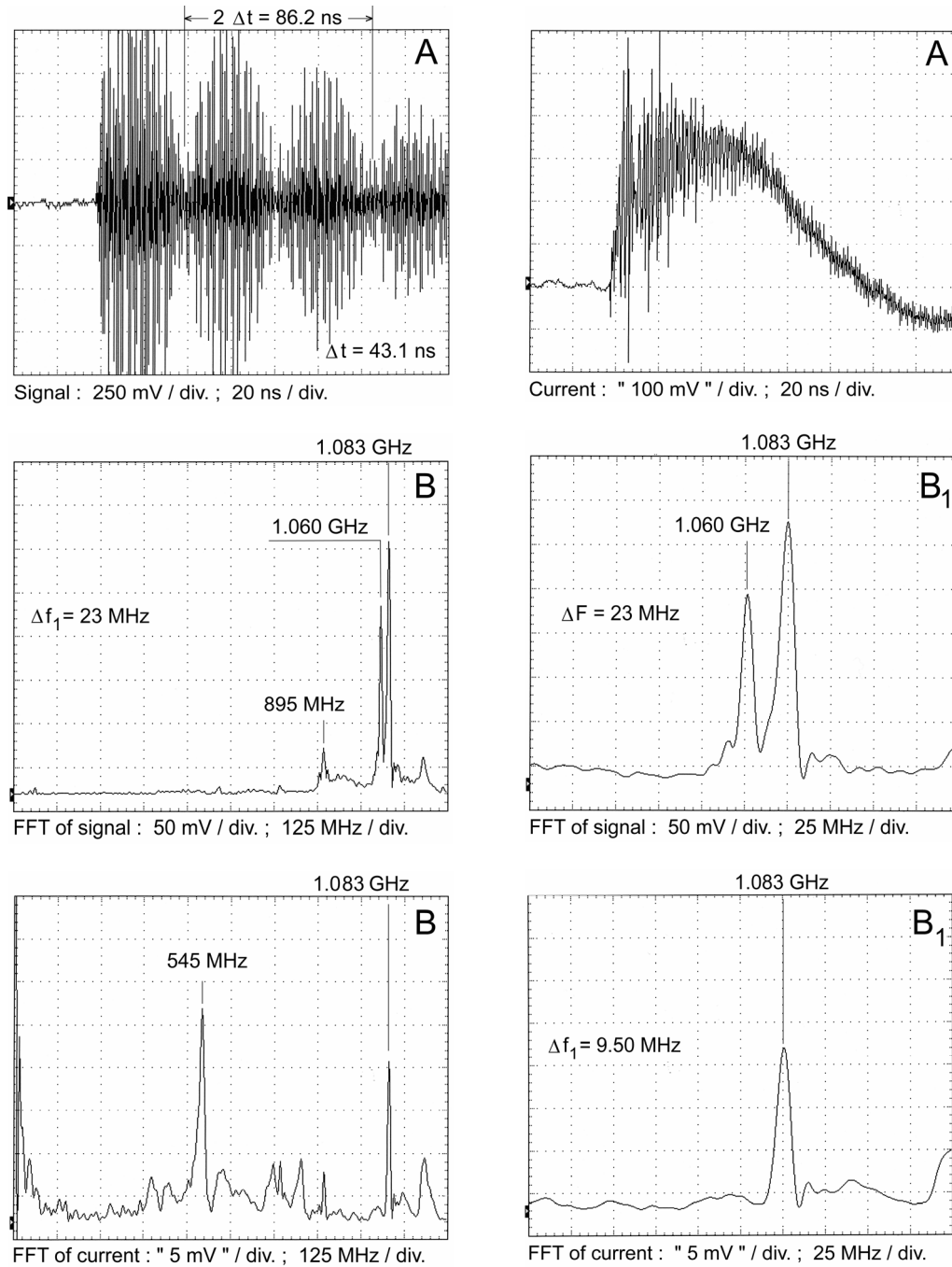


Fig. 10. Microwave emissions generated in argon at 600 torr. The helix was used. Marx generator was charged to ~ 9 kV/stage. The signal in frame A was recorded with B-dot probe and with a low (1.25 GHz) pass filter. Descriptions of traces are as in Fig. 8. Coherence effect is present.

of all the TE modes propagating in the coaxial waveguide. The cutoff wavelength for TE₁₁ mode is

$$\lambda_c = 1/4 \times 1.873 \pi (D + d) \quad \text{when } D = 3d. \quad (4)$$

where D is the diameter of the inner wall of the cylinder and d is the diameter of the circular conductor of the coaxial waveguide. The helix can also approximate the inner circular conductor. For $D = 6$ inch ($=15.24$ cm) and $d = 2$ inch ($=5.08$ cm) used in Fig. 2, (4) yields $\lambda_c = 29.876$ cm, and $f_c = 1.004$ GHz. The experimental data is the frequency range from 1.060 in Fig. 3(a) to 1.083 GHz in Fig. 11.

For a long coil of 50 cm used in [10], the diameter of the inner wall of the cylinder D is 12 inch ($=30.48$ cm). Using the circular plastic tube of 4 inch ($=10.16$ cm) in diameter, the 15 AWG copper wire of 2.9 mm in diameter was tightly coiled on the tube. This makes d to be equal to 10.16 cm plus 2 diameters of 15 AWG copper wire of 2.9 mm. For these dimensions the theoretical cutoff frequency, f_c is 490 MHz. The theoretical value of f_c differs from the experimental value of 472 MHz by 4%. The error could be attributed to the fact that (4) is derived under the condition that $D = 3d$, and in the experimental setup used, we have only $D = 2.75d$.

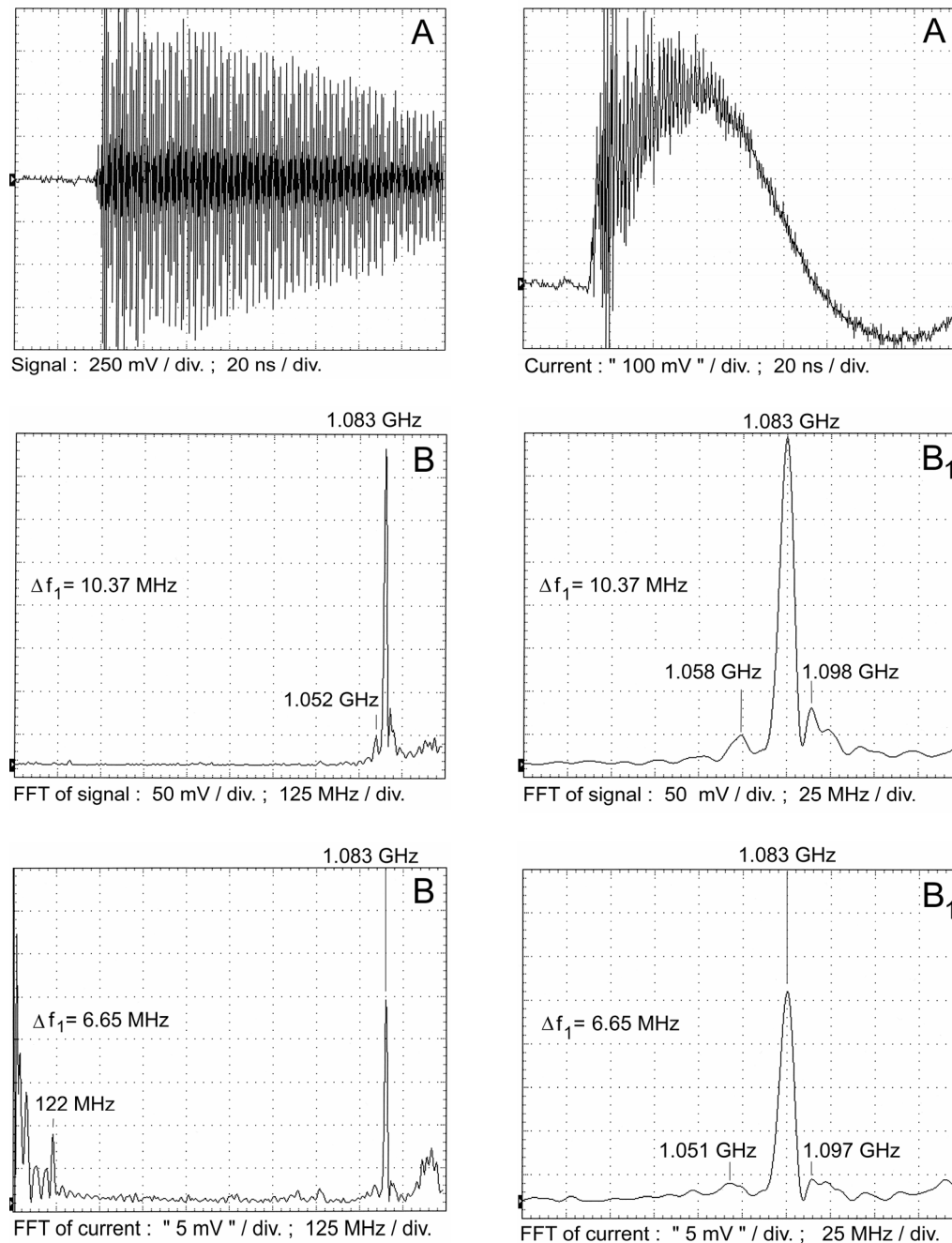


Fig. 11. Microwave emissions generated in argon at 600 torr. The helix structure was used. The signal in frame A was recorded with B-dot probe and using a 1.25-GHz low pass filter. Descriptions of traces are as in Fig. 8. Coherence effect is absent.

For the short coil of 20 cm used in [10], all the dimensions are the same except 24 AWG copper wires of 0.51054 mm in diameter was used. Applying (4), we get $\lambda_c = 60.90$ cm and $f_c = 492$ MHz. In comparison with the experimental value of 483.5 MHz, the error is 1.83%.

To understand the sensitivity of (4), the experiments used to get the data given in Fig. 3(b) were repeated. Instead of the solid aluminum rod of 48.30 mm in diameter, 15 AWG copper wire was tightly coiled on the plastic tube of the same diameter of 48.30 mm. With the solid rod the frequency is 1.090 GHz as shown in Fig. 3(b). By replacing the solid aluminum rod

with the coil tightly coiled on the plastic tube, the frequency becomes 1.046 GHz.

Throughout the research on the microwave generation in air, the coherence effect was the obstacle which inhibited the effort to make significant progress in the research and development.

In this study, further effort was made trying to understand the processes involved. For this reason additional experiments were carried out and the results are shown in Figs. 7–11. The data presented are the summary of a few hundred shots recorded. The most interesting part of these data is the evolution of the emission i.e., what is happening from the onset of

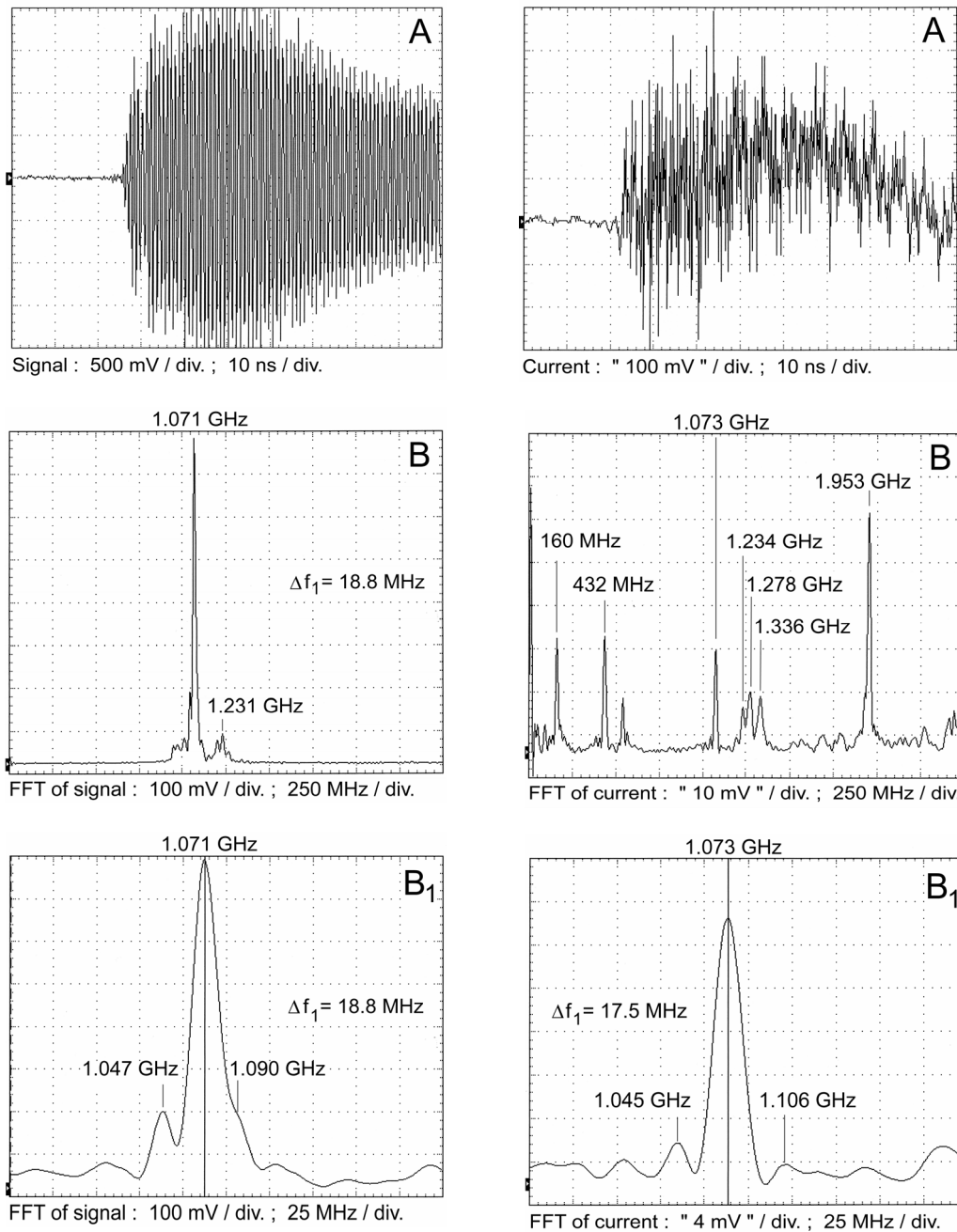


Fig. 12. Microwave emissions generated in air. Solid rod of 2 in (=50.8 mm) in diameter replaces the helix. Marx generator was charged to ~10 kV/stage. The signal in frame A was recorded with B-dot probe and using a 1.25-GHz low pass filter. Other descriptions of traces are as in Fig. 8. Coherence effect is absent.

the emission to the time when Δt starts to be measured (Figs. 6 and 8–10). Studying these processes on the faster (5 ns/div. and 2 ns/div.) time scale, numerous signal lines, and current lines were recorded. The observations of the evolution of the microwave emission points out that these lines are of similar nature as the records given in Fig. 6.

The overall conclusion is that the electromagnetic wave between the cylinder and the helix propagating in the TE_{11} mode [and given by (4)] is not occurring in a synchronized fashion with the radiation wave propagating in the center of the helix. Because of this, it appears we have the interactions

between the different modes, possibly establishing and causing the many frequencies to be formed in the resonant cavity and to have significant variations from shot to shot.

The second important conclusion became evident by making the comparison between Figs. 10 and 11. The coherence effect is due to the interaction between the main frequency at 1.083 GHz and the satellite line at 1.060 GHz in Fig. 10. The coherence effect is absent in Fig. 11 and only the main frequency line at 1.083 GHz was recorded. The surprising fact is that the satellite line is not evident in the FFT of the current trace in Fig. 10.

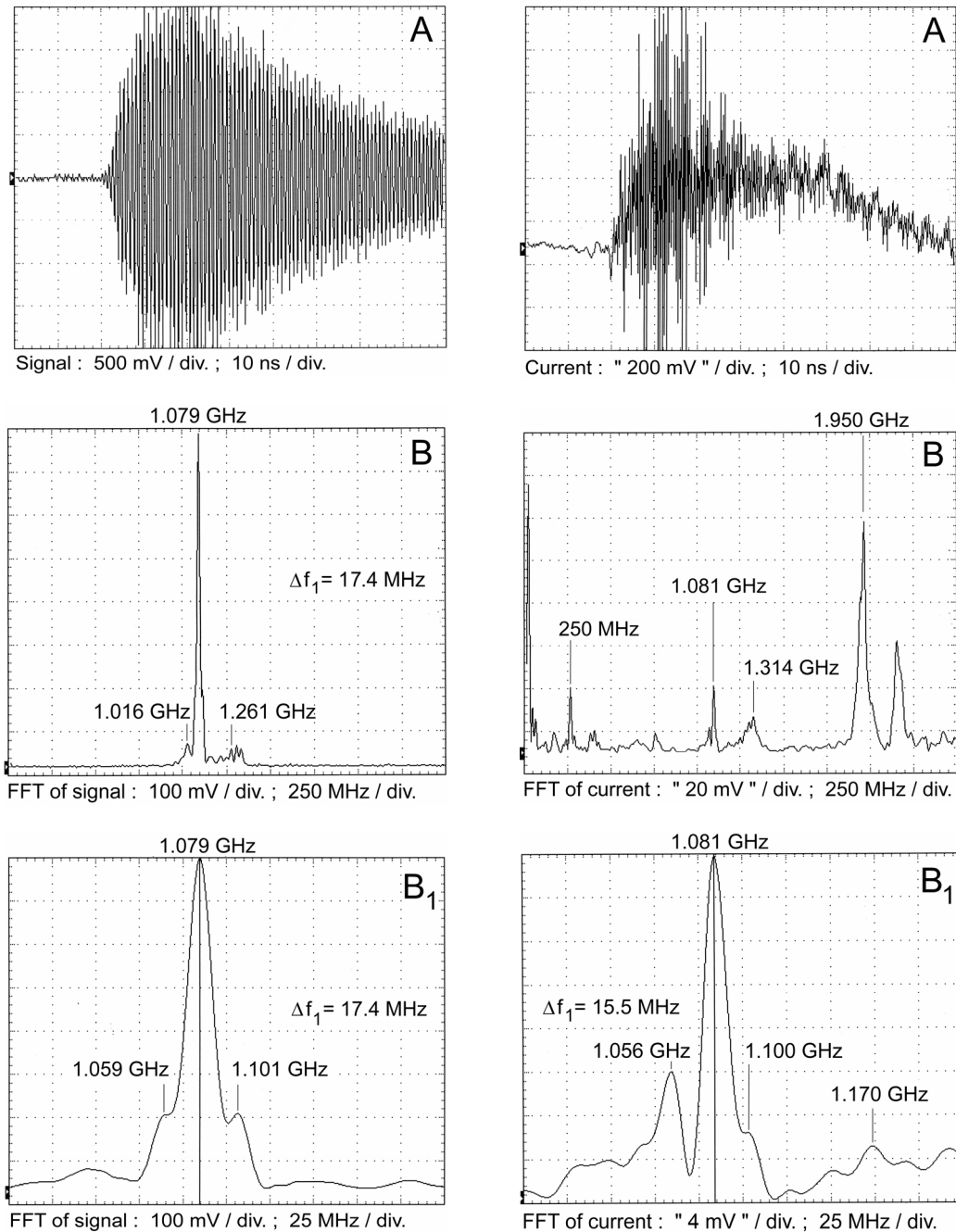


Fig. 13. Microwave emissions generated in air. Solid rod of 2 in (≈ 50.8 mm) in diameter replaces the helix. Marx generator was charged to ~ 10 kV/stage. The signal in frame A was recorded with B-dot probe and using a 1.25-GHz low pass filter. Other descriptions of traces are as in Fig. 8. Coherence effect is absent.

These observations may be explained by the following facts. The CT-1 probe records well the magnetic field of the radiations being generated close to the probe in the space between the cylinder 10 and the helix 11 of Fig. 2. The sensitivity of the probe is decreased for the radiation occurring inside the helix. Second, the FFT trace shown in Fig. 10, frame B₁ is the integral function in time and differs from the FFT observed in a short time period. If we sum up large value many times, also sum up small value many times, it will appear that the sum of small values is difficult to be noticed in comparison to the sum of large values.

To avoid the coherence effect altogether, it is necessary to return to the conditions stated in Fig. 3(b): the solid rod is to replace the helix. The results obtained with the graphite rod of 2 inch (≈ 50.8 mm) in diameter are shown in Figs. 12–14.

In Fig. 3(b), argon was used instead of air and the rod of smaller diameter (≈ 48.30 mm) was applied. The charging voltage of nine-stage Marx generator was adjusted until the minimum variations of the signal's amplitude were obtained. The goal was to examine whether (2) could be confirmed.

The microwave emissions were obtained in air at the frequency of 1.071 shown in Fig. 12 and 1.079 GHz shown

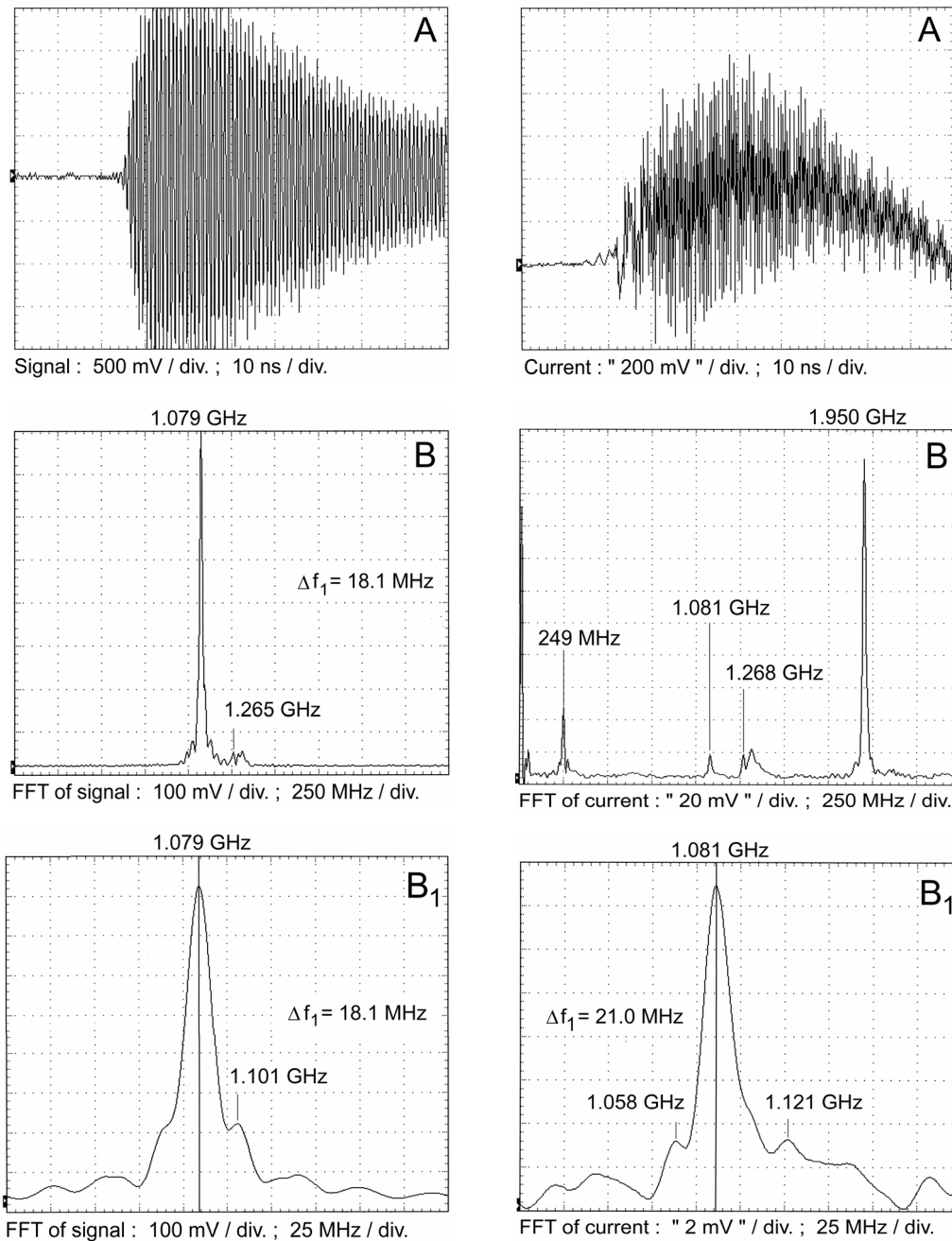


Fig. 14. Microwave emissions generated in air. This data shows some variation from shot to shot with respect to the data given in Fig. 13. The main difference between shots is the shape of the current trace. The signal in frame A was recorded with B-dot probe and using a low (1.25 GHz) pass filter. Other descriptions of traces are as in Fig. 12. Coherence effect is absent.

in Figs. 13 and 14. Using different spacing, the amplitude of the radiation at the frequency close to 1.950 GHz will change. The maximum emission occurs usually at the charging voltage of the nine-stage Marx generator close to 10 kV/stage. By increasing or decreasing the charging voltage from this optimum value, the emission close to 1.079 GHz will fall.

Also, the FFT of the current in Fig. 14, frame B shows that, the peak at 1.081 GHz is 10 times smaller in comparison to the peak at 1.950 GHz.

It should be noted that (4) was found to hold in [10] for the diameter of the inner wall of the cylinder D of 12 inch ($=30.48$ cm) to generate the frequency of 472 MHz

(for a long coil) and 492 MHz (for a short coil). In this study D of 6 inch ($=15.24$ cm) is used and (4) is found to be valid to give the frequency of circa 1 GHz.

If the system is to generate the maser action at the frequency of 1.950 GHz, ($\lambda = 5.385$ cm), (4) points out that the dimensions of the chamber have to be decreased approximately by factor of 2 in comparison to the structure used in this study. For $f = 1.950$ GHz, d should be 1.029 inch ($=2.615$ cm), and $D = 3.088$ inch ($=7.844$ cm).

The peak at 1.95 GHz frequency as reported in [2] in Fig. 2 is just one of the peaks at which the microwave emission does occur in air. The largest peak of the emission

takes place at 7.55 GHz. For the frequency of 7.55 GHz, the (4) gives d of 0.2658 inch ($=6.753$ cm), and $D = 0.7975$ inch ($=2.026$ cm).

Producing the microwave emission at higher frequency i.e., at 7.55 GHz provides the possibility of not only having just a small size system, but also the method to couple the radiation exiting the cavity, by the small size helical antenna to direct the radiation output.

So far, not sufficient attention has been paid to the quality factor Q of the resonant cavity. If the Q of the cavity is large ($Q > 50$), the gain in the current in the cavity/emission at the resonance is high and the cavity discriminates sharply (reject the unwanted frequencies) between the resonant frequency and the frequencies on either side of the resonance.

To determine the quality factor of the system (Fig. 2), it is necessary to consider the exit of the energy from the cavity (represented by the impedance of 377Ω), the energy addition in the cavity due to the maser action (and represented as the resistor of the negative value), the propagation of the wave inside the cavity, the energy loss to the walls and the dimensions of the components in the cavity.

These terms can be approximated by the lump parameters to yield the equivalent series RLC circuit in the vicinity of the resonance. The analysis of the passive series RLC circuit is given in [11].

The conclusions of the preliminary analysis are the following. The quality factor of the radiation line, $Q_r = f/\Delta f_1$ is always larger than the quality factor of the cavity $Q_c = f/\Delta f_c$. For the data shown in Fig. 3(a), it was evaluated that the bandwidth of the cavity Δf_c is close to 50 MHz, whereas the bandwidth of the line Δf_1 is 15.1 MHz at f of 1.060 GHz. When Q_c is of high value, the satellite lines close to the resonance are well attenuated (Fig. 5). When the maser emission is efficient and contributes that the current in the cavity rises to high value, the quality factor of the cavity Q_c resembles that of the commercial klystron tube (i.e., $Q_c \geq 80$).

When the currents/emissions are small, the bandwidth of cavity Δf_c is increased to 100 MHz, making the discrimination of the satellite lines less efficient.

IV. CONCLUSION

In this paper, the microwave generation close to 1 GHz was investigated. Two experimental setups were used. In the first setup, the helix was used. In the second setup, the helix was replaced with the graphite rod of 2 inch ($=5.08$ cm) in diameter. The helix or the rod were placed alternatively in the cylinder of 6 inch ($=15.24$ cm) in diameter.

The self-supporting helix was made using 1/4 inch ($=0.635$ cm) copper tubing and the tubing was coiled on the tube of 2 inch ($=5.08$ cm) in diameter d . According to [12], the pitch for the helix is close to $\lambda/4$ and the wavelength $\lambda = \pi \times d$. These dimensions enable the frequency of the helix to be 1.879 GHz, when the helix is not in the cylinder.

Using the helix, the amplitude of the microwave emission close to 1 GHz is 2 times large in comparison to that found when the solid rod is used. Unfortunately, the probability of

getting always the “good results” with the helix is not satisfactory. This is because in the domain dictated by the quality factor of the cavity, numbers of frequencies are generated and the interactions between the frequencies will lead to the coherence effect. This fact has the consequence that the “good results” became the “bad results” in some shots.

Using the solid rod, the propagation of the electromagnetic wave in the cavity occurs in the TE_{11} mode and the reproducible results are obtained. The system is behaving like a high gain narrow bandwidth amplifier that has a positive feedback and produces the microwave amplification by the stimulated emission of radiation as in the case with the atomic hydrogen maser [4].

The CT-1 probe observes all the radiations being generated in the resonant cavity that are coming from the excited molecules and atoms in the RF and the microwave domain up to the frequency of 3 GHz ($=$ bandwidth of the oscilloscope). The probe measures the magnetic field arising from these electromagnetic radiations.

The FFT trace of the current shown in Fig. 14, frame B indicates that at the frequency of 1.950 GHz, the number of excited molecules is 10 times larger than the number of excited molecules at the frequency of 1.081 GHz.

If the resonant cavity is to be tuned to 1.950 GHz, the inner diameter of the chamber (as well as the solid rod) has to be reduced by factor of 2 in comparison to the cavity designed to get the radiation at 1.079 GHz.

By making the cavity more compact, it becomes practical to add the helical antenna of relatively small dimensions to the exit of the cavity. The helical antenna is to be attached to the partial reflector and the axis of the antenna is to be in the same line as the axis of the cavity. The radiations now exiting the cavity will be coupled to the winding of the helical antenna [13].

If future experiments designed at 1.950 GHz line are successful, this will open further avenues trying to have higher frequency and to make the system even more compact. According to [2], the number of excited molecules in air has the maximum at 7.55 GHz in the microwave domain. This fact means that, theoretically it should be possible to reduce the diameter of the cylinder to about 2 cm.

How far the method suggested can be successful depends on the optimum degree of ionization (produced by the UV radiation and by the electrical field) and in getting a stable uniform discharge between the cylinder and the rod. The problems related to the gas-electrical breakdown between the cylinder and the rod and arc formation are to be avoided. Tailoring and optimization of the discharge parameters is the task ahead. This future work may have some resemblance to the explosively driven (compact) magneto-cumulative generator (MCG) [14].

Some time ago, it was claimed that the MCG of [14] is capable during the detonation of producing the powerful microwave at the frequency range of 10–12 GHz [14]. Many distinguished scientists have disputed such claim. Nevertheless, using the nondestructive method proposed in [10], future experiments offer an inexpensive way to reexamine this discrepancy.

Initially, the system can be energized by the low impedance Marx generator such as the one described in [15] and applied in this study, and later to achieve the burst of the microwave pulses, Nikola Tesla coil generator should be used [10].

By using short rise time Marx generator with the low impedance, the gas discharges may well create conditions where nitrogen laser emission is possible in the future compact coaxial cavity designs. Kindly note that the nitrogen laser operates in the UV domain at the wavelength of 337.1 nm ($f = 8.89910^{14}$ Hz) [16]. The high gain in the nitrogen laser leads to relatively efficient super-luminescent emission even without a laser resonator, not just in nitrogen but even in air [17] (with lower performances). For this reason, the fast photodiode (of rise time < 100 ps) together with the interference filter (337.1 ± 15) nm should be added to get the UV (laser emission) data and supplement the data recorded with B-dot probe in the range from 1 to 10 GHz.

REFERENCES

- [1] M. M. Kekez, "Microwave generation in atmospheric air," *IEEE Trans. Plasma Sci.*, vol. 44, no. 10, pp. 2331–2339, Oct. 2016.
- [2] M. M. Kekez, "Microwave generation in air and vacuum," *IEEE Trans. Plasma Sci.*, vol. 45, no. 2, pp. 235–246, Feb. 2017.
- [3] C. H. Townes. (Dec. 11, 1964). *Production of Coherent Radiation by Atoms and Molecules; Nobel Lecture*, accessed on Jan. 25, 2017. [Online]. Available: <http://nobelprize.org/physics/laureates/1964/towneslecture.pdf>
- [4] H. M. Goldenberg, D. Kleppner, and N. F. Ramsey, "Atomic hydrogen maser," *Phys. Rev. Lett.*, vol. 5, no. 8, pp. 361–363, Oct. 1960.
- [5] P. A. Tipler, *Physics*, 2nd ed. New York, NY, USA: Worth Publishers, Inc., Nov. 1983, pp. 454–456.
- [6] H. Seguin, J. Tulip, and D. McKen, "Ultraviolet photoionization in TEA lasers," *IEEE J. Quantum Electron.*, vol. 10, no. 3, pp. 311–319, Mar. 1974.
- [7] M. M. Kekez, "HPM formation in air and SF₆/Argon mixture," *IEEE Trans. Plasma Sci.*, vol. 41, no. 6, pp. 879–886, Apr. 2013.
- [8] M. M. Kekez, "Interactions between two microwaves generated in air and SF₆/Argon mixture," *IEEE Trans. Plasma Sci.*, vol. 42, no. 6, pp. 1573–1585, Jun. 2014.

- [9] M. M. Kekez, "Are gas discharges capable of generating maser radiation?—Part 1," *IEEE Trans. Plasma Sci.*, vol. 42, no. 11, pp. 3478–3484, Nov. 2014.
- [10] M. M. Kekez, "Magnetocumulative generator as RF/microwave source using Tesla coil method," *IEEE Trans. Plasma Sci.*, vol. 44, no. 4, pp. 617–628, Apr. 2016.
- [11] *Electronics Tutorials: 'Series Resonance Circuit'*, accessed on Jan. 2017. [Online]. Available: <http://www.electronics-tutorials.ws/accircuits/series-resonance.html>
- [12] J. D. Kraus and R. J. Marhefka, *Antennas for All Applications*, 3rd ed. Boston, MA, USA: McGraw-Hill, 2002.
- [13] M. M. Kekez, "Recognizing coherence effects in microwaves," *IEEE Trans. Plasma Sci.*, vol. 41, no. 12, pp. 3599–3603, Dec. 2013.
- [14] A. B. Prishchepenko and M. V. Shchekachev, "The work of impulsive type generator with capacitive load," in *Proc. 7th Int. Conf. Megagauss, Magn. Field Generat. Rel. Topics*, Sarov, Russia, Aug. 1996, pp. 304–307.
- [15] M. M. Kekez, "Efficiency of HPM generation in air," *IEEE Trans. Plasma Sci.*, vol. 40, no. 6, pp. 1668–1671, Jun. 2012.
- [16] A. J. Schwab and F. W. Hollinger, "Compact high-power N₂ laser: Circuit theory and design," *IEEE J. Quant. Electron.*, vol. 12, no. 3, pp. 183–188, Mar. 1976.
- [17] D. Basting, F. P. Schäfer, and B. Steyer, "A simple, high power nitrogen laser," *Opt.-Electron.*, vol. 4, no. 1, pp. 43–49, Jan. 1972.



Mladen M. Kekez was born in 1941. He received the Dipl.-Ing. degree from the University of Belgrade, Belgrade, Serbia, in 1965, and the Ph.D. degree from the University of Liverpool, Liverpool, U.K., in 1968.

From 1971 to 1972 and from 1974 to 2002, he was with the National Research Council of Canada, Ottawa, ON, Canada, where he was involved in the research and development on gas discharges, pulsed-power technology, plasma fusion related experiments, biophysics, and fluid dynamics. From 1972 to 1974, he was with the University of Alberta, Edmonton, AB, Canada, where he was involved in the research and development on the CO₂ lasers. In 2002, he formed the company High-Energy Frequency Tesla Inc., Ottawa. His current research interests include the high-power microwave in air, other gases, and gas mixture.